Marine Pollution Bulletin 221 (2025) 118518

Contents lists available at ScienceDirect

Marine Pollution Bulletin

journal homepage: www.elsevier.com/locate/marpolbul

The continent-to-ocean transfer of rare earth elements in a mediterranean setting: natural processes and anthropogenic emissions

Duc Huy Dang [a,b,*], Gael Durrieu [c], Wei Wang [d], Dario Omanović [e], Cedric Garnier [c], Stephane Mounier [c]

[a] School of the Environment and Department of Chemistry, Trent University, Peterborough, Canada
[b] Water Quality Center, Trent University, Peterborough, Canada
[c] Université de Toulon, Aix Marseille Univ, CNRS, IRD, MIO, Toulon, France
[d] Department of Earth Sciences, University of Manitoba, Winnipeg, Canada
[e] Ruđer Bošković Institute, Division for Marine and Environmental Research, HR-10002 Zagreb, Croatia

ARTICLE INFO

Keywords:
Mass balance
La anomalies
Tb anomalies
River flux
Atmospheric deposition
Particulate loading

ABSTRACT

Despite the ecological and geochemical importance of coastal and estuarine ecosystems, the continental inputs and anthropogenic emissions of trace elements in their global marine budgets are not well constrained due to a lack of comprehensive and inclusive assessment of diverse sources. Here, we investigated two small but representative rivers (Las and Eygoutier) of the Mediterranean Sea to determine the contributions of rare earth elements (REEs) from terrestrial loadings, atmospheric depositions, and anthropogenic emissions within the watersheds and Toulon Bay (France). Both the dissolved and particulate loadings of the rivers significantly increased during intermittent flood conditions relative to base flow. The flow-weighted mean concentrations of dissolved Nd (as a representative REE) ranged from 29 ± 6 and 41 ± 16 ng L^{-1} for the two rivers repectively, while the time-weighted mean particulate concentrations (TWMC) were 8.0 ± 3.4 and 18.8 ± 6.3 mg kg^{-1}. Similarly, TWMCs of atmospheric depositions were 13.3 ± 1.8 and 23.7 ± 4.0 mg kg^{-1} for dry and wet conditions. Atmospheric depositions and fluvial particulate loadings are the primary input and output within the watershed, while river dissolved fluxes, porewater diffusion, and atmospheric depositions are the primary external sources of Nd to the water column. Furthermore, we observed significant La anomalies in the dissolved and atmospheric fractions while the discharge of treated wastewater is a significant REE input to the bay, marked by Tb anomalies. Overall, these results suggest considering small but typical rivers, rather than focusing solely on major fluvial systems, to gain a more comprehensive understanding of the transport and fate of REEs at the continent-to-ocean interface.

1. Introduction

Coastal environments comprise narrow transition zones that connect continental and marine ecosystems. Despite the limited surface area (<20 % of Earth's surface), coastal zones host 45 % of human population, 75 % of megacities with more than 10 million inhabitants, and provide 90 % of global fisheries and 25 % of global biological productivity (Crossland et al., 2005). Estuarine and coastal systems are also significant sites of highly dynamic biogeochemical processes that transform terrestrial materials conveyed by riverine systems into the oceans. These interfaces, therefore, have a substantial impact on projections of marine primary production and the global marine budgets of the elements (Gao et al., 2023; Xu et al., 2023). For some trace elements and isotopes that received decades of investigation through national and international programs, their input and output fluxes are balanced with well-characterized sources and sinks (Conway et al., 2021; Elbaz-Poulichet et al., 2001; Tagliabue and Weber, 2024). Other elements, e.g., rare earth elements, still have their unbalanced marine mass budgets despite numerous applications as important geochemical tracers (Arsouze et al., 2009; Conway et al., 2021; Dang et al., 2022b; Garcia-Solsona and Jeandel, 2020; Laukert et al., 2017; Rousseau et al., 2015; Xu et al., 2023).

Rare earth elements (REEs) include 15 lanthanides, Sc and Y. They are widely used as tracers for continental inputs, present and past ocean

* Corresponding author at: School of the Environment and Department of Chemistry, Trent University, Peterborough, Canada.
E-mail address: huydang@trentu.ca (D.H. Dang).

https://doi.org/10.1016/j.marpolbul.2025.118518
Received 12 May 2025; Received in revised form 23 July 2025; Accepted 28 July 2025
Available online 4 August 2025

circulation, redox processes and anthropogenic emissions (Bellefroid et al., 2018; Dang et al., 2022a; Hatje et al., 2016; Kulaksiz and Bau, 2007; Laukert et al., 2017). The most common sources of REEs in the ocean are riverine fluxes, atmospheric deposition, and dissolution of sediment particles, while the dominant sink consists of settling particles (Arsouze et al., 2009). However, missing fluxes (Arsouze et al., 2009; Garcia-Solsona and Jeandel, 2020) and differential geochemical behaviours of REEs associated with distinct geochemical and environmental features over temporal and spatial scales are commonly reported. For example, re-dissolution rates of REEs from riverine particles of the Amazon River have been estimated to be ca. 0.94 % (Rousseau et al., 2015), while no re-dissolution was observed in the high latitude estuaries of the Laptev Sea (Laukert et al., 2017). Nevertheless, the dissolution of REEs from particles in the Amazon River was more recently attributed to the contribution of the nearby Para River (Xu et al., 2023). Furthermore, the salt-induced coagulation of REEs in the estuary of the St. Lawrence River was also not observed under ice-covered conditions (near-conservative behaviour) despite significant removal in ice-free seasons (Dang et al., 2022b). These observations point toward the need to investigate small rivers instead of strictly focusing on major fluvial systems (Brown et al., 2020), contrasting environmental conditions (Dang et al., 2022b; Xu et al., 2023), and less conventional and accessible ecosystems, e.g., mangrove (Dang et al., 2021) and high-latitude (Laukert et al., 2017), to further constrain the inputs of these elements to the global ocean.

The Mediterranean Sea offers a unique non-conventional system with contrasting environmental conditions, providing an opportunity to investigate continental fluxes of elements into the ocean. It is located between the temperate and subtropical zones, with unique meteorological features of hot and dry summers, contrasting with wet falls and springs. In addition to extensive damming of rivers, such conditions significantly reduced river discharge, further exacerbating the variations in river flow between the base-flow seasons and intermittent floods (Laubier, 2005). Extensive studies on trace element geochemistry have been conducted on major rivers of the Mediterranean Sea basins, including the Rhône, Po, Nile, and Ebro (Elbaz-poulichet, 2005; Ollivier et al., 2010). Although they represent a significant fraction of water discharge to the sea, these main rivers do not represent the typical Mediterranean rivers, which have comparatively smaller watersheds and are subject to flash floods that induce drastically different environmental transport and fates of trace elements (Elbaz-poulichet, 2005).

Here, we investigate the Las and Eygoutier Rivers (southeast of France) as typical small rivers of the Mediterranean coast, also referred to as "oueds", that are characterized by low water discharge under dry conditions but high peaks during flood events (Dufresne et al., 2020; Nicolau et al., 2012). We collected river water over two years under base-flow conditions and at a higher temporal resolution during a flood event. A similar approach was used to collect suspended particles and atmospheric depositions (under both wet and dry conditions). Surface seawater was also collected from the bay. This extensive and inclusive set of samples enables an in-depth assessment of REE fluxes from the watersheds to the bay, shedding light on the natural geochemical processes governing REE fates and their anthropogenic emissions.

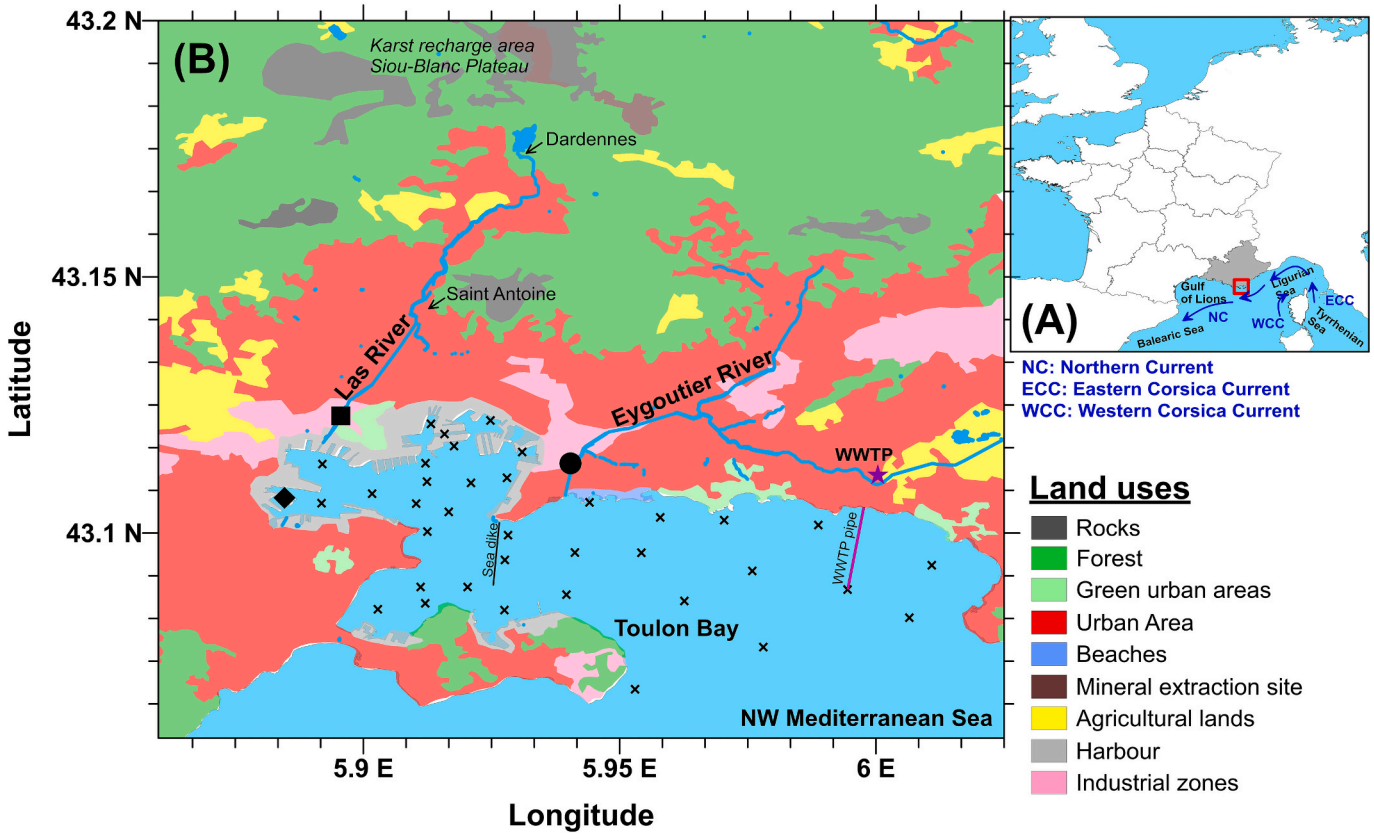

Fig. 1. (A) Map of France with the study site (red squares) and the major oceanic currents. (B) The watersheds of the Las and Eygoutier Rivers, and Toulon Bay. Land uses are obtained from the Corine Land Cover (2012) database accessed through the French Geoportal (https://www.data.gouv.fr/en/datasets/corine-land-cover-occupation-des-sols-en-france/, updated on April 20, 2024). The sampling location for river water and particulate matter from the Las and Eygoutier Rivers are indicated by the filled squares and circles, respectively. Atmospheric depositions are collected from La Seyne-sur-Mer (filled diamond). Seawater was collected from 36 stations within Toulon Bay (crosses). The purple star indicates the wastewater treatment plant (WWTP) Amphora discharging treated wastewater 1800 m away from the coast into the large bay through a submarine pipeline (purple line). (For interpretation of the references to colour in this figure legend, the reader is referred to the web version of this article.)

2. Materials and methods

2.1. Study site

The hydrology and water chemistry of the Las River (8 km) are complex due to the influence of karst springs and urbanization within the watershed (60 km^2) (Durrieu et al., 2023). The two main karst springs (Dardennes and Saint-Antoine, Fig. 1B) are recharged from the Siou-Blanc limestone plateau and constitute an important feature in the upstream region of the river. Additionally, the downstream section is significantly impacted by runoff in the urban area of approximately 14 km^2 (Dufresne et al., 2020). On the other hand, the Eygoutier River (16 km) has a watershed area of 70 km^2, with its upstream section mainly influenced by agricultural and industrial activities, and the downstream area characterized by high urbanization (Nicolau et al., 2006). Both rivers are typical Mediterranean oueds, characterized by significant variations in water discharge between the dominant dry conditions and temporary flood events, e.g., 0.01 to 37.5 $m^3\ s^{-1}$ in the Las River (Dufresne et al., 2020) and 0.01 to 11 $m^3\ s^{-1}$ in the Eygoutier River (Nicolau et al., 2006).

The two rivers represent the primary freshwater sources in Toulon Bay, a semi-enclosed bay in the northwestern Mediterranean Sea (Fig. 1). The bay can be divided into a small bay (9.9 km^2, average depth of 12 m, volume of $90 \times 10^6\ m^3$) and a larger one (24 km^2, max depth of 50 m, volume of $760 \times 10^6\ m^3$), separated by a sea dike. The former receives water from the Las River, while the Eygoutier River discharges into the large bay. Toulon Bay is highly urbanized, with significant tourism, military and aquaculture activities (Dang et al., 2015; Tessier et al., 2011). The large bay also receives treated wastewater from a wastewater treatment plant (WWTP, with a capacity of 115,000 inhabitants) through a submarine pipeline (Fig. 1B); close to $5 \times 10^6\ m^3$ of wastewater is treated annually (Métropole Toulon Provence Méditerranée, 2019).

Overall, the region is characterized by a typical Mediterranean climate. Rainfall is, however, highly variable annually in terms of total precipitation: 525 mm in 2017, 1289 mm in 2018, and 1033 mm in 2019 (data from www.historique-meteo.net for Toulon). Nevertheless, the common trend is that most rain occurred from October to April (**Fig. S1**).

2.2. Sampling and sample treatment

A complete description of the sampling protocol for all sample types was previously provided (Durrieu, 2022; Durrieu et al., 2023). The samples consist of filtered river and seawater, suspended particles collected by sediment traps under both dry and flooded conditions (base flow and during a flood event), and atmospheric depositions (in both dry and wet conditions). It is important to note that all sampling devices were pre-cleaned following a strict protocol for ultra-trace elements, which consists of rinsing with (i) ultra-pure water (18.2 MΩ cm) three times, (ii) 10 % HNO_3 (analytical grade) over 24 h (sampling bottles) or one week (large bottles for atmospheric depositions), and (iii) ultra-pure water (18.2 MΩ cm) three times before (iv) a final rinse with the samples.

River water and particles were collected 900 m at the river mouths (Fig. 1B); all samples collected were freshwater with an average specific conductivity of 0.5 ± 0.3 mS cm^{-1} (n = 57). Water samples were collected during the base flow (18 from the Eygoutier River and 21 from the Las River) and floods (11 samples from each river) from January 2017 to February 2019. For the base flow, a large volume (2 to 4 L) of river water was collected from the stream into pre-cleaned FEP (fluorinated ethylene propylene) bottles. During a flood event on October 10, 2018 (94 mm of precipitation), we adopted a high-resolution sampling strategy (hourly from 11 h AM to midnight: 11 samples for each river). Due to the high variability in water flow during floods, we collected composite samples of 60-mL aliquots taken every 10 min over one hour or every 20 min over two hours, depending on the river flow, in 500 mL FEP bottles. A rainwater sample was also collected. All samples were immediately filtered (0.2 μm, cellulose acetate, Sartorius) and acidified with 0.5 % suprapure HNO_3.

A sediment trap (Phillips et al., 2000) was deployed at the same locations on the two rivers to collect suspended particles. This approach is well adapted for low-flow and small streams over a long period to obtain a time-integrated signature (Durrieu et al., 2023). Depending on meteorological conditions, the traps were deployed between 3 and 41 days from March 2017 to February 2019, i.e., 22 periods for Eygoutier and 26 for the Las River. Because of the brief nature of the flood event, we collected composite suspended particulate matter from hourly sampled water (900 mL) composed of six 150-mL aliquots (collected every 10 or 20 min). The composite waters were filtered through a 0.2 μm cellulose acetate filter (Sartorius) to collect suspended particles at a higher resolution than the particle trap. The filters or 100 mg of particles were mineralized in *aqua regia* using microwave digestion (Milestone, UltraWAVE ECR); the procedure has been described by (Durrieu et al., 2023).

Atmospheric depositions were collected at Ifremer (French Institute for Ocean Science, La Seyne-sur-Mer, Fig. 1B). Wet depositions (rain) were sampled using an automatic collector that triggers the cap during precipitation events to channel the rain into a 27 cm diameter funnel, which in turn directs the rain into a 5-L perfluoroalkoxy (PFA) bottle. This design allows the collection of up to 87 mm of precipitation. From November 2019 to June 2020, we collected 12 events of wet depositions with durations from 2 to 11 days of accumulated rain (0.1 L to 3.2 L). Dry depositions were collected using a separate collector into a 20 L bucket; the device closes during rain events. Due to the limited material deposited during dry periods, the duration of each sampling was extended from one to two months (33 to 64 days). At the end of each period, we added 1.5 L of ultra-pure water to the bucket, shook it for 30 min and transferred the solutions to a 2 L FEP bottle. Both wet and dry depositions (in 1.5 L of ultrapure water) were collected on 0.2 μm cellulose acetate filters (Sartorius). The filters were digested using a procedure similar to that of suspended particles.

We also collected surface seawater from 36 stations of Toulon Bay on June 16, 2022 (Fig. 1B). A detailed sampling protocol is provided in Dang et al. (2015). Briefly, the samples were collected in 125 mL FEP bottles, filtered through a 0.2 μm cellulose acetate syringe filter (Sartorius), and acidified with Suprapur HNO_3 (Merck). The samples were pre-concentrated on Nobias resin according to the protocol described by (Dang et al., 2022b; Ma et al., 2019) for elemental analysis.

2.3. Analyses, quality assurance and quality control

Elemental analysis of filtered river water, digestate of suspended particles and atmospheric deposition, and pre-concentrated seawater was performed by ICP-MS (8800 Agilent Technologies) at the Water Quality Centre (Trent University) following a protocol previously described (Dang et al., 2022b). Analytical recovery was verified using two certified reference materials (CRMs): river waters SLRS-6 and AQUA-1 from the National Research Council of Canada (NRCC). The CRMs and blank samples were used to bracket every ten samples. A detailed comparison between measured and certified or consensus concentrations of water CRMs is provided in **Table S1** and **Figs. S2 A-D**. We also included the sediment CRM PACS-2 (NRCC) to assess elemental recovery from microwave digestion (**Table S2**). The recovery averaged 98 % for REEs. We also included blank filters in digestion batches; the REE background in these filters (ranging from 0.02 ng for Lu to 0.73 ng for La) was ca. 2 % of average REE concentrations in atmospheric deposition samples and < 0.2 % of average REE concentrations in suspended particle samples.

It is important to note that we directly analyzed the river waters using ICP-MS without preconcentration; Tm and Eu concentrations in some samples were close to or below the instrument's detection limits (0.1 to 1 ng L^{-1}). Thulium is the least abundant REE (1 % of La abundance in the upper continental crust, UCC (Rudnick and Gao, 2003)),

while Eu has limited reactivity with O_2 to form EuO^+ (eight times lower than the La oxide formation yield (Sugiyama, 2022)). We have, therefore, screened the measured concentrations against the detection limits and removed unreliable data, including Eu concentrations in all river waters and Tm concentrations in the samples collected during the flood event.

For the analysis of pre-concentrated seawater, we utilized a high-sensitivity desolvating nebulizer (Apex-Q, Elemental Scientific; more details in (Ma et al., 2019)). QA/QC was checked using an in-house seawater standard traceable to seawater CRM CASS-6 (NRCC) (Dang et al., 2022b); this sample was collected from Middle Cove Beach (Newfoundland and Labrador, Canada), conditioned and calibrated according to the protocol described by (Wang et al., 2022). More information is detailed in **Table S3** and **Fig. S2, *E*-F**. Blank columns were also included in preconcentration batches, and the average background REE levels (ranging from 0.8 fg of Lu to 1.4 pg of La) were approximately 0.5 % of the minimum REE concentrations in seawater samples.

Dissolved organic and inorganic carbon (DOC and DIC) were analyzed using a TOC-V analyzer (Shimadzu); the detailed analytical procedure and QA/QC were previously described (Durrieu et al., 2023). Similarly, the river flows were determined using a limnometer and a pressure sensor; data on the Las River had already been published (Durrieu et al., 2023).

2.4. Data analysis

Rare earth element concentrations were normalized against UCC values (Rudnick and Gao, 2003) to obtain smooth REE patterns, which will be referred to as REE_{UCC}. While there are numerous normalization materials (e.g., chondrite, Post-Archean Australian Shale, North American Shale Composite) to obtain REE patterns (Rétif et al., 2023), it is challenging to find a single material that consistently covers several environmental media targeted by this study (e.g., dissolved, particulate and atmospheric fractions, river vs marine waters). For this reason, we elected to use UCC as a universal material rather than a specific geological standard like shale.

The anomalies of La, Gd and Tb were calculated using the following equations.

$$La \Big/ La^* = \frac{La_{UCC}}{\frac{Pr^3_{UCC}}{Nd^2_{UCC}}} \quad (1)$$

$$Gd \Big/ Gd^* = \frac{Gd_{UCC}}{\frac{1}{2} \times (Sm_{UCC} + Dy_{UCC})} \quad (2)$$

$$Tb \Big/ Tb^* = \frac{Tb_{UCC}}{\frac{1}{2} \times (Eu_{UCC} + Ho_{UCC})} \quad (3)$$

The anomalies of La and Gd are calculated based on commonly accepted approaches (Dang et al., 2022b; Wang et al., 2020). However, Tb/Tb* can be calculated based on the Eu, Gd, Dy or Ho as the adjacent REEs. Both Eu and Gd are problematic because of their own anomalies in natural samples. Here, we chose to calculate Tb anomalies based on Eu and Ho for seawater samples because of the limited Eu anomalies in this particular matrix, while some natural or anthropogenic Gd anomalies might exist, especially in wastewater.

The concentrations of the elements in suspended particles were also used as inputs for principal component analysis (PCA) using a Matlab code (Dang et al., 2015).

3. Results and discussion

3.1. River water chemistry

Despite their proximity, the two river water systems have distinct total dissolved solids (TDS) content, revealing different weathering processes; TDS average values under base-flow conditions in the Eygoutier River (16.1 ± 2.6 mEq L^{-1}, $n = 18$) are significantly higher ($p < 0.0001$) than those of Las River water (10.2 ± 2.2 mEq L^{-1}, $n = 21$). The different Na/(Na + Ca) ratios (0.26 ± 0.02 in Eygoutier vs 0.17 ± 0.05 in Las River) in the Gibbs diagram (Fig. 2A) also indicate the more substantial influence of evaporation and crystallization in the Eygoutier River watershed. However, during the flood event, the higher TDS values in Las (5.7 ± 2.6 mEq L^{-1}, $n = 11$) relative to Eygoutier (2.5 ± 0.7 mEq L^{-1}, n = 11) indicate a quick response time and a strong influence of runoff from urban and industrial areas of its catchment. This is also reflected in the increase in DOC concentrations during the flood event to 4.7 ± 2.0 mg L^{-1} (n = 11, Las River) and 8.8 ± 3.6 mg L^{-1} (n = 11, Eygoutier River) relative to the values of 1.1 ± 0.7 mg L^{-1} (n = 21) and 3.0 ± 2.1 mg L^{-1} (n = 18) for the base-flow average values, respectively.

Because of the karstic and calcareous rocks of the local watersheds, carbonate ions constitute a major part of the TDS (34.2 ± 10 %, $n = 61$); DIC/Ca ratios in all samples vary between the 1:1 and 2:1 lines (Fig. 2B), while Mg/Ca remains at a constant molar ratio of 0.24 ($r^2 = 0.98$, $n = 62$, **Fig. S3A**). This ratio is slightly lower than the characteristic Mg/Ca ~ 0.33 (i.e., equal weathering of calcite and dolomite), suggesting a slightly stronger contribution from calcite relative to dolomite (Szramek et al., 2007). We related Na/Ca to Mg/Ca ratios in the water samples (Fig. 2C) and compared them to the three end-members (carbonate, silicate, and evaporite rocks) that have been defined for the Rhône River in southern France (Ollivier et al., 2010). The base-flow samples align between the signatures of silicate and carbonate rocks, while the samples during the flood event shift toward the evaporites (red arrow in Fig. 2C). Nevertheless, this shift toward higher Na/Ca values can also indicate growing anthropogenic contributions, as the increase in Na, Cl, K, and other anions (such as sulphate and nitrate) is often associated with human activities. During the flood event, we observed an increase in Na, K, sulphate and Cl relative to Ca and DIC (**Fig. S4**), indicating either the contribution from the rain end-member (increased Na/(Na + Ca) to ~0.8, Fig. 2A) or other anthropogenic sources, e.g., sewage, runoff, fertilizers. In fact, there is a preferential release of K over Na as the K/Na ratio rises from 0.06 in the base flow in the Eygoutier River to 0.16 under flood conditions (**Fig. S3B**). Given the substantial occurrence of farmlands in the Eygoutier River watershed, this observation is coherent with the land uses, highlighting agricultural activities as significant sources of nutrients to the aquatic systems.

Furthermore, high water flow during floods might also mobilize other elements from the watershed; both Th/U and Rb/Sr ratios increase by almost two orders of magnitude during the flood (**Fig. S3C**), although Th and Rb are considered less mobile during erosion and transport compared to U and Sr, respectively (Gaillardet et al., 2003). Such mobilization could be associated with increased leaching of dissolved organic carbon from the watershed, the colloidal fractions (Chabaux et al., 2003), and desorption processes from suspended particles or atmospheric deposition (Gilbert et al., 2023). The mobility of poorly soluble Th in surface water can also be enhanced by complexation with oxyanions (particularly sulphate) and organic complexes (Langmuir and Herman, 1980), as well as contributions from groundwater or deep rock-water interactions in the critical zone (Gilbert et al., 2023). We did not observe a significant trend between Th, sulphate, or organic matter (**Fig. S5, A and B**) that would indicate Th mobilization from surficial soil systems. However, the strong correlation between Th and Be ($r^2 = 0.88$, $n = 61$, **Fig. S5 C**) would suggest a release from the subsurface environment, e.g., groundwater or leaching of Be from the bedrock (Bolan et al., 2023); this hypothesis seems plausible given the karstic nature of

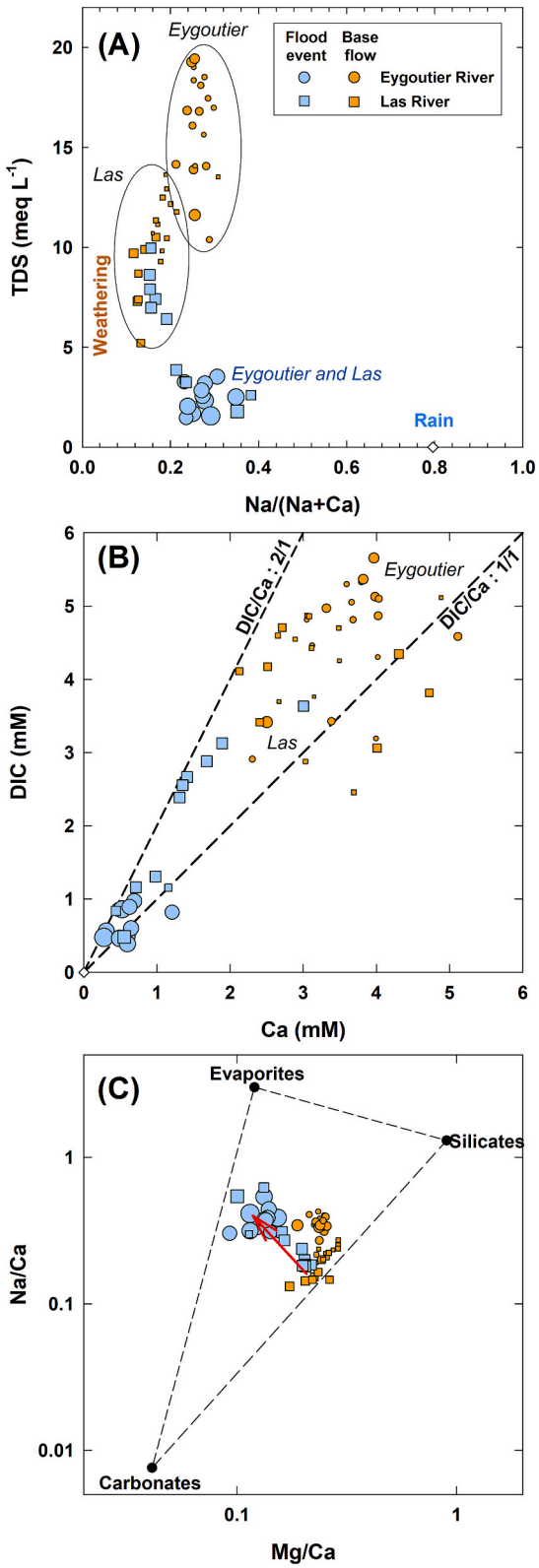

Fig. 2. The Gibbs diagram (A) as well as the relationships between dissolved inorganic carbon (DIC) vs. Ca (B), and Na/Ca vs. Mg/Ca (C) of the Las (squares) and Eygoutier (circles) Rivers. The rainwater collected during the flood event is shown by the open diamond. Orange symbols indicate samples collected during the base flow, and blue symbols show samples collected during the flood event. Symbol sizes are proportional to river flow (ranging from 0.07 to 144 $m^3\ s^{-1}$). (For interpretation of the references to colour in this figure legend, the reader is referred to the web version of this article.)

the local geology. Nevertheless, the origins of these elements cannot be well constrained given the complex nature of these interactions involving atmospheric, hydrogeological, and pedological processes.

3.2. REE concentrations and anomalies

3.2.1. River waters

We hereafter present the results of Nd as a representative REE as Nd concentrations and isotopes have been extensively reported and used as a geochemical tracer and in ocean mass balance budget. This enables a comparison of this dataset to a comprehensive literature on other river and marine systems globally.

Neodymium dissolved concentrations show significant variations over the two years of investigation (Fig. 3). There is no clear temporal variation trend observable for the monthly monitoring data of base flow conditions; the average Nd concentrations are, however, significantly higher ($p = 0.003$) in Eygoutier (7.6 ± 3.7 ng L^{-1}, $n = 16$) than Las River (4.2 ± 2.6 ng L^{-1}, $n = 21$). This observation also applies to the flood event (39.7 ± 5.8 ng L^{-1}, $n = 10$ vs 28.6 ± 13.0 ng L^{-1}, $n = 11$; $p = 0.02$) (Fig. 3**, B and C**). These elevated Nd concentrations relative to the rainwater collected during the flood event ([Nd] $= 1.7 \pm 0.9$ ng L^{-1}) highlight local inputs of Nd within the watersheds. This observation is consistent with a trend in dissolved Nd concentrations related to water flow and suspended particulate matter (SPM; Fig. 4**, A and B**). However, the robust correlation between Nd and Th (Fig. 4C) is intriguing, as it suggests a subsurface contribution (groundwater or springs, see Section 3.1). This observation is consistent with the recently established mass balance model for the Northwestern Mediterranean Sea, as submarine groundwater discharges contribute an equal amount of REEs to the ocean as the riverine flux, i.e., 10–11 % of the marine mass budget (Garcia-Solsona and Jeandel, 2020).

Furthermore, the assessment of REE patterns (**Fig. S6**) reveals an overall change in the geochemical behaviours of REEs between the base-flow and flood conditions. The overall UCC-normalized patterns during base flow are typical of the "seawater-like", with higher UCC-normalized concentrations of heavy REEs relative to light REEs. This behaviour has been extensively discussed in the literature and associated with the preferential sorption of light REEs on reactive surfaces while the heavy REEs remain in solution by complexing with various dissolved ligands, including carbonate (Byrne and Li, 1995; Dang et al., 2022b; Lee and Byrne, 1993). During the flood, the patterns (**Fig. S6, B and D**) became flat and closer to those of suspended particulate matter (**Fig. S6, *E*-H**), which could be associated with a rapid exchange between the dissolved and particulate fractions and less available dissolved ligands (carbonate) to bind the heavy REEs, making them more available for sorption. Between the base flow and the flood, DIC concentrations decreased from 55.1 ± 9.7 mg L^{-1} ($n = 18$) to 8.1 ± 2.4 mg L^{-1} ($n = 11$) for the Eygoutier River and from 49.0 ± 8.6 mg L^{-1} ($n = 21$) to 24.2 ± 12.1 mg L^{-1} ($n = 11$) for the Las River.

We also observed anomalies of La and Gd in the river waters (Fig. S5, A-D). Significant anomalies of La and Gd have been reported in rainwater in Japan and China (La and Gd: Shimamura et al., 2007; Zhu et al., 2016), in urban air in Spain (La: Moreno et al., 2010) and in atmospheric particles (PM10) in Texas (Bozlaker et al., 2013). Gadolinium anomalies are well-documented in urban rivers globally and are associated with the discharge of treated or untreated wastewater, as well as the use of gadolinium in contrast agents for magnetic resonance imaging (Kümmerer and Helmers, 2000; Rabiet et al., 2009). Therefore, the Gd anomalies observed in both Las and Eygoutier systems are not unexpected given the urban settings and dense populations with major hospital centers. Gd/Gd* values under base-flow conditions seem to be higher (7.7 ± 4.1 and 5.6 ± 3.4 for Las and Eygoutier Rivers, respectively) than the rain event (2.5 ± 1.0 and 2.9 ± 1.1, respectively), which suggests a dilution effect with uncontaminated waters.

Unlike Gd anomalies, La anomalies are more locally reported and mainly associated with specific sources, e.g., cracking catalysts for

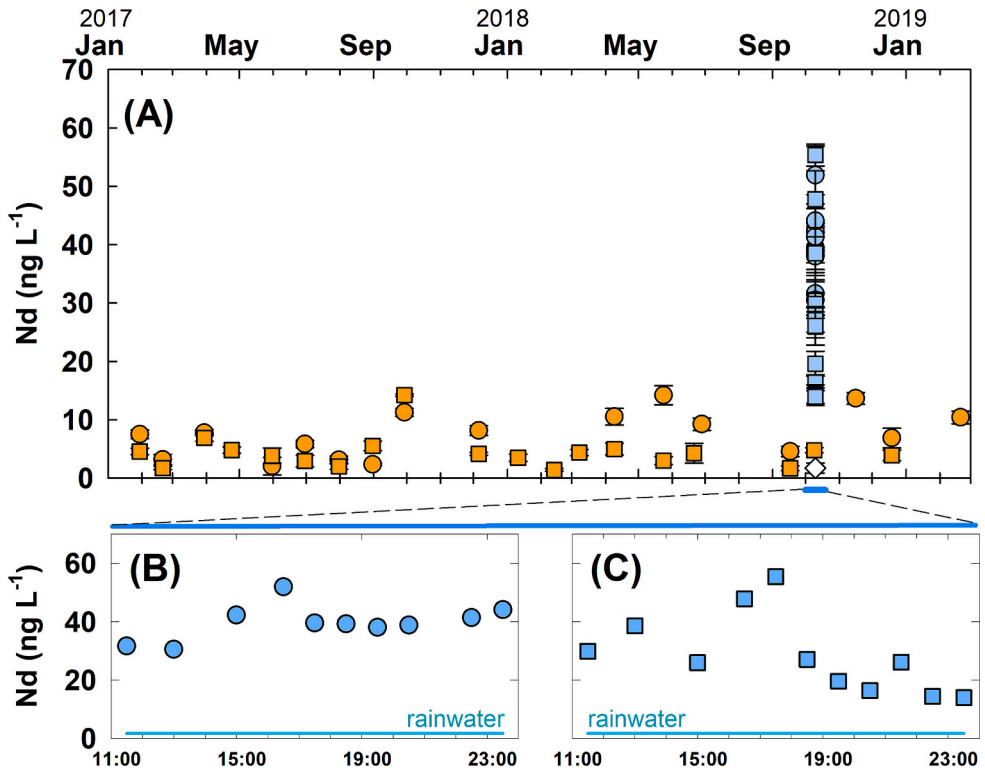

Fig. 3. (A) Temporal variations in dissolved Nd concentrations under base-flow conditions (orange symbols) and during the flood event (blue symbols) of the Eygoutier (circles) and Las (squares) Rivers. Panels B (Eygoutier River) and C (Las River) show the hourly resolution variations in Nd concentrations during the flood event of the two rivers relative to rainwater (cyan lines). (For interpretation of the references to colour in this figure legend, the reader is referred to the web version of this article.)

petrol refining as it has been traced from a point source along the Rhine River (Kulaksiz and Bau, 2013) or La-based fertilizer that has been extensively utilized in China (Zhu et al., 2016). We observe La/La* up to 140 in Las River water under base-flow conditions (Fig. 5A). Such elevated values (up to 160) were reported in the Rhine River near the discharge of industrial effluent associated with petroleum refining catalysts (Kulaksiz and Bau, 2013). We also processed the data on REE concentrations reported in PM2.5 emitted from petroleum refinery in the Houston (Texas, USA) area (Kulkarni et al., 2007) and found significant La/La* of up to 130 in both industrial and residential locations away from the source. If we exclude the two values of La/La* > 100 in our river water samples, there is no significant difference between the rivers and seasons, with La anomalies ranging from 1 to 24.1, suggesting a significant enrichment of La in the river system.

While Nd concentrations in the rainwater (1.7 ± 0.9 ng L^{-1}) collected during the flood event were significantly lower than the river water (Fig. 3, **B and C**), it was not the case for La (**Fig. S7, B and C**). The concentrations of La in the rainwater were 40 ± 0.7 ng L^{-1} and higher than 60 % of the river samples reported in this study (37 out of 59). This observation suggests an atmospheric source of La, as has been the case in Houston (Kulkarni et al., 2007). Coincidentally, one of the largest petrochemical complexes in France is located 73 km northwest of Toulon and is owned by a company similar to the one at the Houston site. While this is not a direct indication of a point source explaining the La anomalies, emissions from this site can be carried by the northwesterly wind (Mistral) to Toulon as one of the dominant wind directions (40 %) (Dufresne et al., 2014). Nevertheless, La concentrations in river water during the flood event remain equal to or higher than those in rainwater (**Fig. S7, B and C**), revealing additional sources of mobilization. Further studies will be required to constrain the sources of La anomalies in this region.

3.2.2. *Suspended particles and atmospheric depositions*

Temporal variations in the concentrations of La (Fig. 6A) and other REEs, e.g. Nd (Fig. 6B) in suspended particles, are consistent over time and with limited La anomalies (La/La* <2, Fig. 6C). It is also important to note that La anomalies are not observed in suspended particles of the Eygoutier River (La/La* = 0.93 ± 0.04, n = 34 for all particles), confirming that the sources of La enrichment relative to other REEs are not of lithogenic origins, at least in this larger watershed less impacted by industrial activities and intense urbanization. Lanthanum concentrations in particles under base-flow conditions are relatively constant over the two years, and the average concentrations are higher in Eygoutier River (23.4 ± 5.6 mg kg^{-1}, n = 22) than the Las River (11.7 ± 4.0 mg kg^{-1}, n = 26). During the flood event, La concentrations increased to 32.6 ± 3.9 mg kg^{-1} (n = 12) in Eygoutier and 21.5 ± 9.9 mg kg^{-1} (n = 10) in Las River. Most of these values are well below the concentrations in UCC (30 mg kg^{-1}) and Post Archean Australian Shale (38.2 mg kg^{-1}) (McLennan, 2001; Rudnick and Gao, 2003). We also did not observe any anthropogenic Gd anomalies (Gd/Gd* < 1.2, n = 70) in the particle traps or during the flood event. Furthermore, the PCA also indicates robust correlations between REEs, lithogenic elements (e.g., Al, K, Ti, Mn, Fe), and trace elements (e.g., Li, Ga, Ge, Rb, As, Th) (**Fig. S8**). The anti-correlation between this cluster of elements and Ca indicates that the principal carrier phases of trace elements, including REEs, are mainly clays (Al) or oxides (Fe and Mn) in the two watersheds.

On the other hand, La concentrations in wet (33 ± 21 mg kg^{-1}, n = 12) and dry (28 ± 27 mg kg^{-1}, n = 6) depositions remain in similar ranges as the suspended particles in river systems. Nevertheless, there was one event in January–February 2020 where La concentrations reached above 80 mg kg^{-1} (Fig. 7A). Such a spike in concentrations was not observed for Nd (Fig. 7B), but there is a similar increase in the concentrations of Cr, Mn, Sr, Zr, Ba and U (**Fig. S9**). This differential behaviour from that observed in suspended particles (**Fig. S8**) would suggest a specific atmospheric source of these elements. Furthermore,

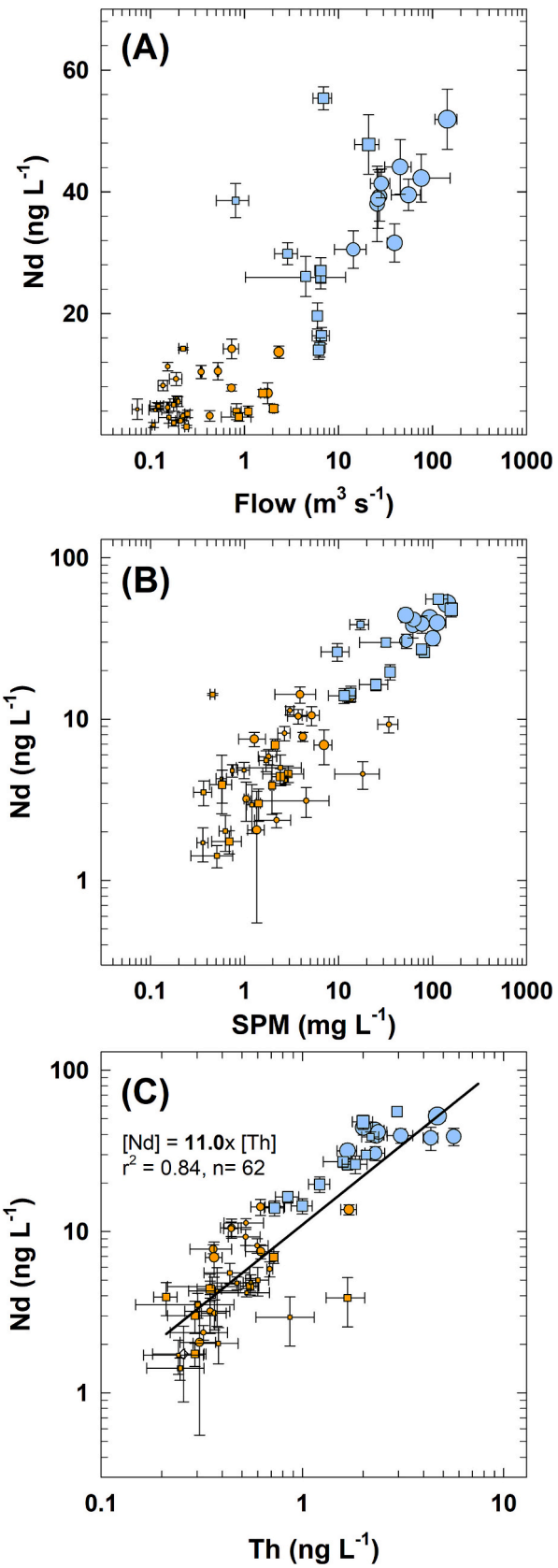

Fig. 4. Relationships between dissolved Nd concentrations and river water flow (A), suspended particulate matter (SPM, B) and dissolved Th concentration (C). See the legend of Fig. 2 for symbol shapes and colours. Symbol sizes are proportional to river flow (ranging from 0.07 to 144 $m^3\ s^{-1}$).

this event also exhibits elevated La anomalies in both wet and dry depositions (La/La* of 3.5 and 4.4) relative to the background values of 1.2 ± 0.1 ($n = 16$) (Fig. 7C).

In summary, the limited anomalies of La in suspended particles would constrain that the La contamination observed in the dissolved fractions of the two river systems is likely associated with an atmospheric source.

3.2.3. REEs in seawater

The overall UCC-normalized REE patterns (**Fig. S10**) in seawater are consistent with the conventional seawater profiles. The concentrations are also consistent with previously reported data for surface water of the central Mediterranean Sea (10–20 m below the surface): our average Nd concentrations of 3.1 ± 1.3 ng L-1 ($n = 36$) compared to reported concentrations of 3.7 ± 0.4 ng L^{-1} (n = 10) (Censi et al., 2004). However, higher Nd concentrations (>4 ng L^{-1}) can be observed at stations 2, 8, 9, 32, 52, 36 and 34 (Fig. 8A) corresponding to the Toulon civil marina (station 2), the French Navy base (stations 8, 9) as well as the discharge point of the WWWT submarine pipeline (stations 32, 34, 36, 52). Very low Nd concentrations were, however, observed at the core of the French Navy base (stations MIS, 3, 4, 6 ext), where the highest La anomalies were recorded (Fig. 8B). We also observed Tb anomalies in UCC-normalized REE patterns (**Fig. S10**, with Tb/Tb* values up to 3.3); the highest values were recorded at the discharge location of the WWTP (Fig. 8C).

Anomal Tb concentrations when measuring Tb at the *m/z* of 159 ($^{159}Tb^+$) might be associated with polyatomic inferences of Nd isotopes, i.e., $^{143}Nd^{16}O^+$ or $^{142}Nd^{16}O^1H^+$. Nevertheless, because we measured Tb with a mass shift from m/z 159 ($^{159}Tb^+$) to 175 ($^{159}Tb^{16}O^+$), the Tb anomalies we observed are unlikely related to inference. An interference from Nd on this elevated m/z of 175 would be caused by a cascade of double oxide formation from $^{143}Nd^+$ and $^{142}Nd^+$ to $^{143}Nd^{16}O^+$ and $^{142}Nd^{16}O^1H^+$ (1st ICP/MS quadrupole at m/z of 159), then to $^{143}Nd^{16}O^{16}O^+$ and $^{142}Nd^{16}O^{16}O^1H^+$ (the 2nd quadrupole at m/z of 175). We have conducted a test on the interference of $BaOO^+$ on EuO^+ in natural river water, and with increasing Ba/Eu ratios up to 15,000; these double oxide interferences are unlikely to affect the measurement of REEs (Dang and Wang, 2024). It is, however, important to note that this test was conducted on an Agilent 8900 ICP-MS with N_2O as the reaction gas, which is more efficient in forming oxides (Sugiyama, 2022). Furthermore, high Tb/Tb* ratios were recorded in samples with low Nd/Tb ratios (**Fig. S11**), thereby eliminating the hypothesis of polyatomic interferences from Nd on Tb isotopes. It is also important to note that we eliminated most environmental matrices by preconcentrating REEs through the Nobias resin (using 1 M HNO_3 as the elution matrix), further reducing the risks of analytical inferences (e.g., chlorides).

These results confirm relatively unimpacted background concentrations of REEs in the surface seawater of Toulon Bay, except for some point sources associated with the nautical and military activities as well as treated wastewater. While the extensive contamination of Toulon Bay sediments and surface water has been demonstrated for inorganic elements and organic compounds (Dang et al., 2015; Guigue et al., 2017; Layglon et al., 2020; Tessier et al., 2011), data are not available for rare earth elements. Furthermore, the Tb anomalies in natural samples are rarely reported, although Tb is an REE with extensive applications, e.g., fluorescent lamps and displays, electro-optical devices and magnets (Andrade et al., 2023). The fact that the Tb emissions are linked to wastewater is somewhat plausible but requires further assessment to ascertain the specific sources of Tb.

The scientific community only recognizes a few specific anthropogenic REE anomalies, as they are strictly associated with a specific and well-constrained source (e.g., La, Sm, Gd). New anomalies require a substantial level of caution. A first non-conventional anthropogenic REE anomaly (Lu) was recently reported in the Isère and Rhône Rivers (Lu/Lu* up to 20.5) and confirmed to be related to wastewater treatment plant effluents (Alemu et al., 2025). The authors excluded the

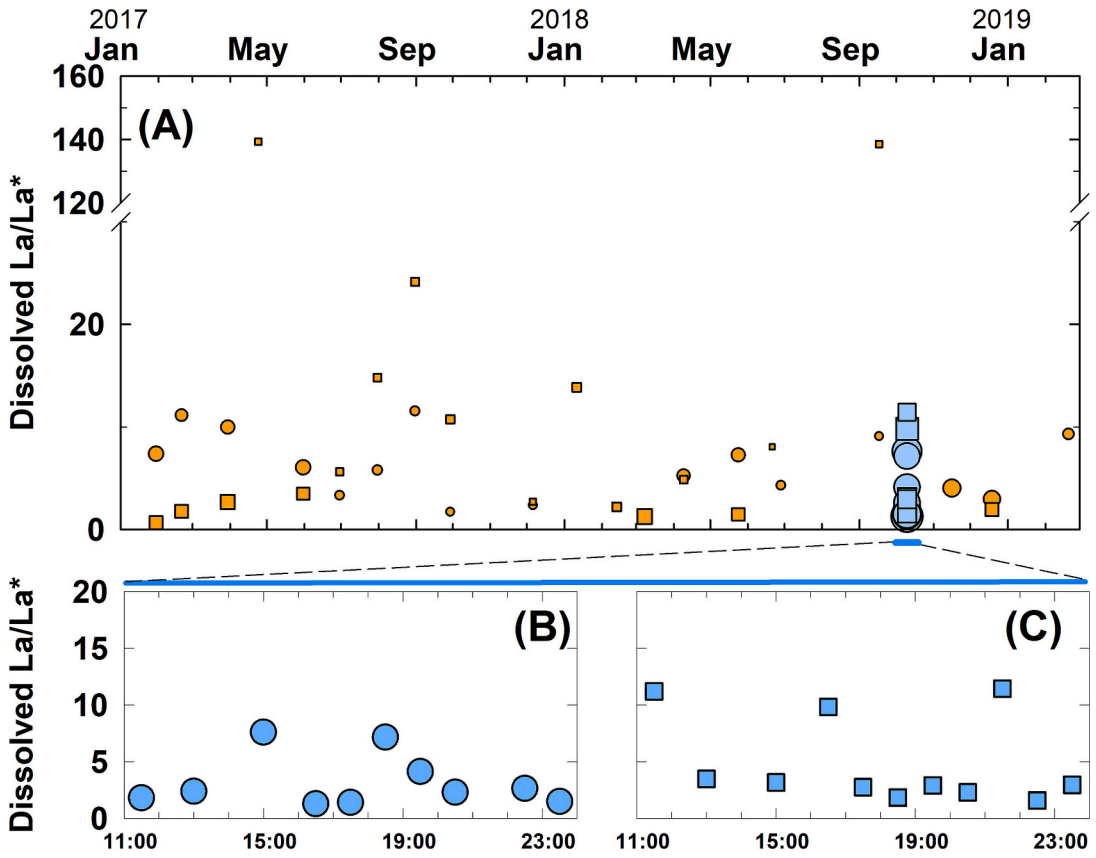

Fig. 5. (A) Temporal variations in La anomalies in river water under base-flow conditions (orange symbols) and during the flood event (blue symbols) of the Eygoutier (circles) and Las (squares) Rivers. Panels B (Eygoutier River) and C (Las River) show the hourly resolution variations in La anomalies during the flood event of the two rivers. Symbol sizes are proportional to river flow (ranging from 0.07 to 144 $m^3\ s^{-1}$). (For interpretation of the references to colour in this figure legend, the reader is referred to the web version of this article.)

hypotheses of analytical artifacts or radionuclides, as Lu could be used in nuclear medicine. They suggested that the positive Lu anomalies were related to a highly stable Lu compound that persists through the wastewater treatment process. We also utilized a pre-concentration approach to eliminate potential polyatomic interferences on Tb. The fact that Tb anomalies were observed near the outlet of a WWTP is intriguing as it is consistent with Lu anomalies reported in the Isère River. While further validation is warranted, the extensive use of individual REEs in a broad spectrum of technological innovations may lead to more widespread microcontamination of specific REEs, resulting in new anomalies that could serve as specific tracers for these new sources.

3.3. REE fluxes and mass balance budgets

3.3.1. Fluxes of Nd within the watershed

We first empirically computed a flow-weighted mean concentration ($FWMC_{dis.}$) of dissolved Nd to take into consideration the substantial variability in water flows (q_i) over time (t_i), and dissolved REE concentrations (C_i). The number of observations (n) was 24 for Eygoutier and 28 for the Las River, including the base flow samples and the flood event of October 10, 2018.

$$FWMC_{dis.} = \frac{\sum_1^n C_i \times t_i \times q_i}{\sum_1^n t_i \times q_i} \quad (4)$$

Dissolved Nd FWMC in the Eygoutier and Las Rivers are 41 ± 16 ng L^{-1} and 29 ± 6 ng L^{-1}, respectively. These concentrations remain lower than the global FWMC of 129 ng L^{-1} (Dang et al., 2022b) or 136 ± 9 ng L^{-1} (Xu et al., 2023). Nevertheless, these Nd concentrations are consistent with the river concentration values of 41 ng L^{-1} used in ocean mass balance models (Goldstein and Jacobsen, 1987) and the median concentration of freshwater ([Nd] = 30 ± 37 ng L^{-1}, $n = 11$) that has been recently compiled (Pereto et al., 2024).

Previous long-term (462 days, 2012–2014) hydrological monitoring of the Las River system documented a mean discharge of 1.66 $m^3\ s^{-1}$ with a range from 0.01 to 37.5 $m^3\ s^{-1}$ (Dufresne et al., 2020); this is also consistent with our data, with an average flow ($\overline{q_w}$) of 0.82 $m^3\ s^{-1}$ and a range from 0.01 to 29 $m^3\ s^{-1}$ (Durrieu, 2022). Similarly, the average flow of the Eygoutier River in base flow was estimated to be 0.014 $m^3\ s^{-1}$ but could be up to 100 $m^3\ s^{-1}$ (Nicolau et al., 2012), which remains consistent with our data: range from 0.09 to 209 $m^3\ s^{-1}$ and $\overline{q_w}$ of 1.2 $m^3\ s^{-1}$ (Durrieu, 2022). Accordingly, the annual dissolved load of Nd can be extrapolated by multiplying the dissolved Nd FWMC with the average flow $\overline{q_w}$ of each river and a correction factor (to convert s to year).

$$Q_{dis.} = FWMC_{dis.} \times \overline{q_w} \times CF \quad (5)$$

The annual dissolved loads $Q_{dis.}$ are 1.5 ± 0.6 kg yr^{-1} and 0.8 ± 0.2 kg yr^{-1} for the Eygoutier and Las Rivers, respectively. These values can be normalized against the watershed surface areas (Table 1) to determine the specific dissolved loading flux of Nd of 0.011 ± 0.002 and 0.026 ± 0.010 kg $km^{-2}\ yr^{-1}$, which remain consistent with the ranges of values reported for the Garonne River (France) for Nd from 0.003 to 0.013 kg $km^{-2}\ yr^{-1}$ despite significantly elevated the river flows (300–750 $m^3\ s^{-1}$) and watershed surface area (57,000 km^2) (Lerat-Hardy et al., 2019).

We employed a similar approach to determine the annual particulate loading of Nd from the two river systems. The average concentrations of particulate Nd require, however, a different calculation because of longer integrating times to collect particles in the trap (Fig. 6A), e.g., 1 to 2 h for the flood event but up to 41 days during the base flow. The

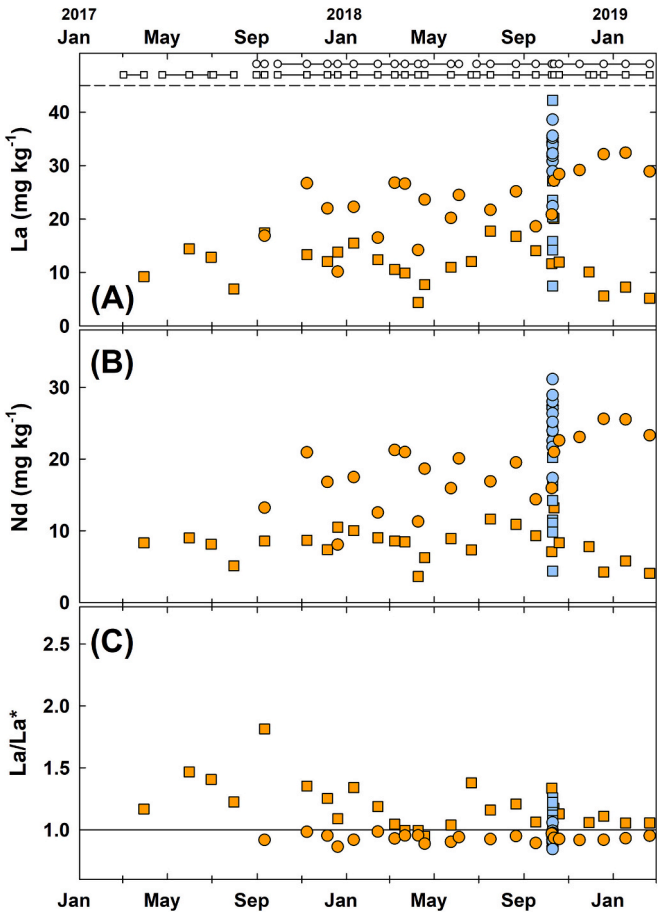

Fig. 6. (A) Temporal variations in La concentrations (A), Nd concentrations (B) and La anomalies (C) in suspended particulate matter under base-flow conditions (orange symbols) and during the flood event (blue symbols) of the Las (squares) and Eygoutier (circles) Rivers. The upper panel in A shows the integration time for each sample collected by particle traps deployed in the Las (open squares) and Eygoutier (open circles) Rivers. (For interpretation of the references to colour in this figure legend, the reader is referred to the web version of this article.)

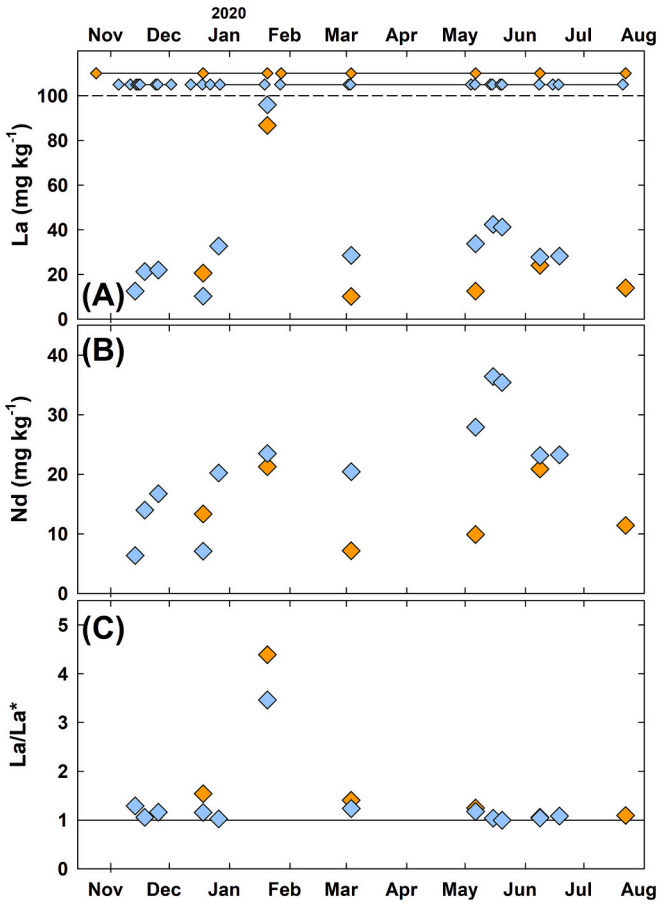

Fig. 7. (A) Temporal variations in La concentrations (A), Nd concentrations (B), and La anomalies (C) in atmospheric depositions under dry (orange) and wet (blue) conditions. The upper panel in A shows the integration time of each sample sampled by atmospheric deposition collectors. (For interpretation of the references to colour in this figure legend, the reader is referred to the web version of this article.)

average is then calculated based on a temporal resolution, i.e., a time-weighted mean concentration ($TWMC_{part.}$).

$$TWMC_{part.} = \frac{\sum_1^n C_i \times t_i}{\sum_1^n t_i} \quad (6)$$

The $TWMC_{part.}$ of particulate Nd are 18.8 ± 6.3 and 8.0 ± 3.4 mg kg^{-1} for the Eygoutier and Las Rivers. The annual particulate loadings of Nd ($Q_{part.}$) of the two respective rivers were determined by multiplying $TWMC_{part.}$ by the loadings of suspended particulate matter (q_{SPM} of each river (Table 1), yielding to $Q_{part.}$ of 38.5 ± 12.9 and 4.2 ± 1.8 kg Nd yr^{-1} for the Eygoutier and Las River, respectively.

The TWMCs of Nd in atmospheric depositions were also calculated using eq. 6: $TWMC_{dry}$ of 13.3 ± 1.8 mg kg^{-1} and $TWMC_{wet}$ of 23.7 ± 4.0 mg kg^{-1}. The atmospheric particles were weighted to determine specific deposition rates of q_{dry} = 9.3 g m^{-2} y^{-1} and q_{wet} = 4.7 g m^{-2} yr^{-1} (Durrieu, 2022). By multiplying the atmospheric deposition rates and Nd TWMCs, $Q^S_{atm.}$ of Nd were consistent between the two conditions, i.e., 0.12 ± 0.02 mg Nd kg^{-1} m^{-2} yr^{-1} of dry deposition and 0.11 ± 0.02 mg Nd kg^{-1} m^{-2} yr^{-1} of wet deposition. Within the watershed of the Las (60km^2) and Eygoutier (70 km^2) Rivers, the Nd depositions under both dry and wet conditions were, therefore, estimated at 14.1 ± 2.4 kg Nd yr^{-1} and 16.4 ± 2.8 kg Nd yr^{-1}, respectively.

Overall, although fluxes of the most significant pathways of Nd cycling within the two watersheds can be computed, Nd budgets within the watershed cannot be reasonably constrained because of low spatial sampling resolution and missing biogeochemical processes, e.g., (im) mobilization during particle suspension and contributions from sedimentary systems. However, atmospheric deposition seems to be the primary input of REEs into the watershed, and particulate loadings constitute a significant output of REEs.

3.3.2. *Neodymium fluxes in Toulon Bay*

While our sampling stations are not designed for watershed mass balance, they are well-positioned to determine Nd fluxes from the watershed to Toulon Bay. Inputs of Nd to Toulon Bay include the dissolved, particulate loadings from the watersheds (including the atmospheric deposition onto the watersheds) but also atmospheric deposition on the bay, submarine groundwater discharge, diffusion from the sediments, inputs of seawater from the Northern Current (Fig. 1A) and emissions from the WWTP.

The total annual dissolved loading fluxes of Nd from the Las and Eygoutier Rivers are 2.3 ± 0.6 kg yr^{-1} (Table 1). Nevertheless, estuarine processes, e.g., salt-induced coagulation, are well known to effectively remove (average of 70 %) dissolved REEs (Dang et al., 2022b; Goldstein and Jacobsen, 1988; Xu et al., 2023). Therefore, effective dissolved loading fluxes by rivers ($F_R^{eff.}$) can be determined by multiplying the dissolved loading flux of Nd by ϕ, the effective factor to consider estuarine removal processes (ϕ = 30 %, (Dang et al., 2022b)), i.e., 0.7 ± 0.2 kg yr^{-1}.

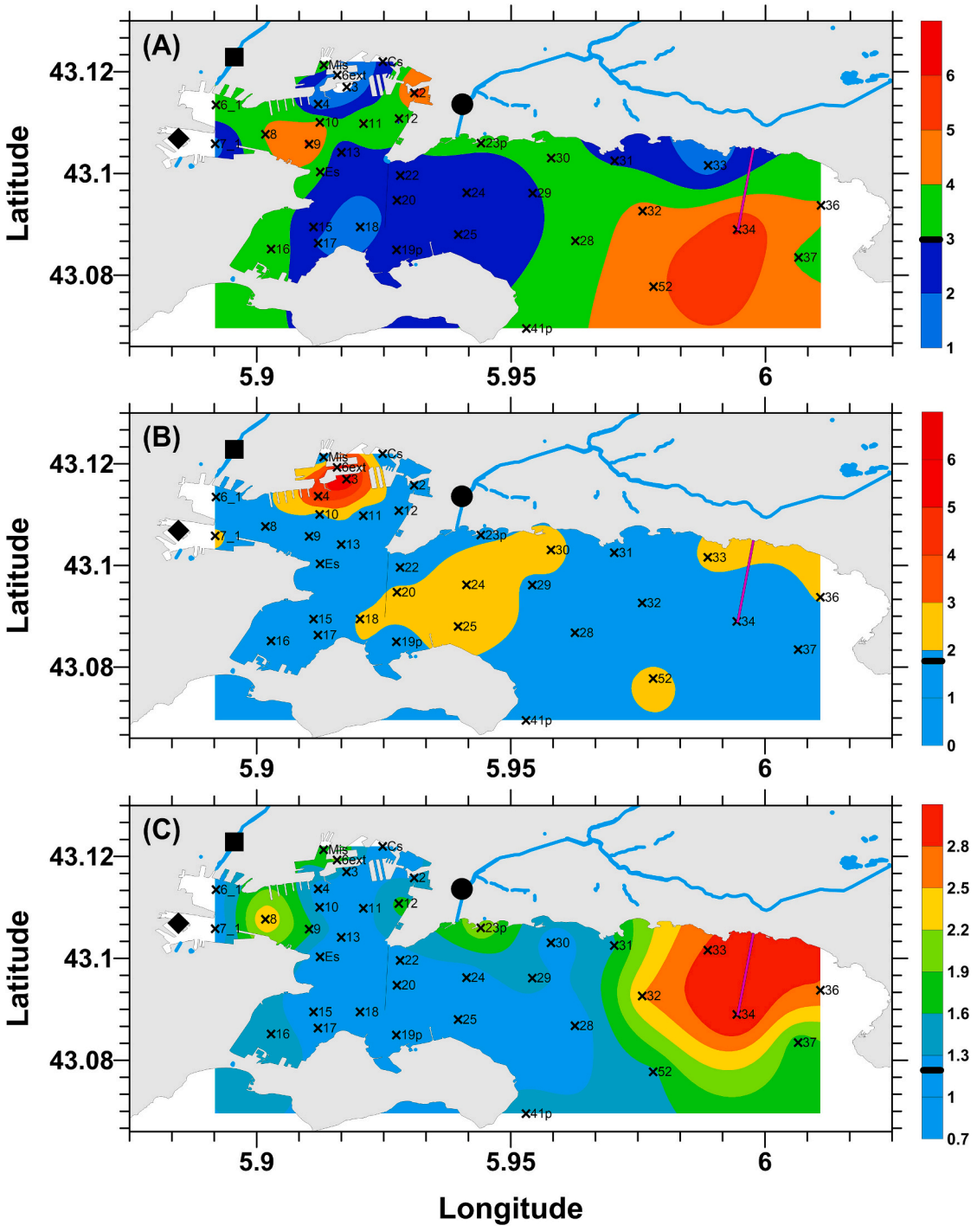

Fig. 8. Map of dissolved Nd concentrations (A), La anomalies (B) and Tb anomalies (C) in Toulon Bay surface seawater. The horizontal black bars on the colour legend indicate the median values.

Submarine groundwater discharge (SGD) is also a significant input of REEs identified in several coastal regions (Garcia-Solsona and Jeandel, 2020; Kim and Kim, 2011). Neodymium concentrations in SGD to the Gulf of Lions have been quantified to be 7.7 ± 0.1 ng L^{-1} (Garcia-Solsona and Jeandel, 2020), and SGD along the French Mediterranean coastline are estimated to be ~2 % of local river inputs (Bejannin et al., 2017), or 0.04 m^3 s^{-1} for the Toulon Bay region. The inputs of Nd to Toulon Bay from SGD (F_{SGD}) are, therefore, estimated to be 0.01 kg yr^{-1}.

The specific loading fluxes of atmospheric depositions (wet and dry) in Toulon (0.23 ± 0.04 kg Nd km^{-2} yr^{-1}) can also be multiplied by the surface area of Toulon Bay (32 km^2), to determine the atmospheric deposition of Nd. However, it has been determined that 1–3 % of REEs can be dissolved from marine atmospheric dust into seawater (Greaves et al., 1994). The atmospheric flux of Nd in Toulon Bay ($F_{atm.}$) was calculated to be 0.16 ± 0.08 kg yr^{-1} by integrating this mobilization factor (2 ± 1 %). Similarly, Rousseau et al. (2015) estimated that only 0.94 ± 0.25 % of Nd particulate flux from the river ($Q_{part.}$) is released to the dissolved Nd pool when these particles enter the estuary. We can, therefore, determine the effective particulate loading flux ($F_{part.}$) to be 0.004 ± 0.001 kg yr^{-1}. This flux is minimal and consistent with recent evidence indicating an insignificant contribution of Nd released from particles (Xu et al., 2023).

Table 1
Summary of main input parameters and outputs of mass balance fluxes of Nd in the watersheds of the Las and Eygoutier Rivers. Numbers in parentheses indicate the number of observations. The errors are calculated as the standard deviation of the dataset with n observations or as propagated errors through the empirical calculations.

			Watershed	
		Abbreviation	Las River	Eygoutier River
Watershed surface area (km^2)			60	70
Dry deposition rate* (July 2019–July 2020, g m^{-2} yr^{-1})		q_{dry}	9.3	
Wet deposition rate* (July 2019–July 2020, g m^{-2} yr^{-1})		q_{wet}	4.7	
Average water flow* (July 2017–March 2019, m^3 s^{-1})		$\overline{q_w}$	0.8	1.2
Particulate loadings* (July 2017–March 2019, kg yr^{-1})		q_{SPM}	520 × 10^3	2050 × 10^3
Average concentrations	Dry deposition (mg kg^{-1})	$TWMC_{dry}$	13.3 ± 1.8 (6)	
	Wet deposition (mg kg^{-1})	$TWMC_{wet}$	23.7 ± 4.0 (12)	
	Dissolved fraction (ng L^{-1})	$FWMC_{dis.}$	29 ± 6 (28)	41 ± 16 (24)
	Particulate fraction (mg kg^{-1})	$TWMC_{part.}$	8.0 ± 3.4 (36)	18.8 ± 6.3 (33)
Loading flux (kg Nd yr^{-1})	Atmospheric deposition	$Q_{atm.}$	14.1 ± 2.4	16.4 ± 2.8
	Dissolved loading	$Q_{dis.}$	0.8 ± 0.2	1.5 ± 0.6
	Particulate loading	$Q_{part.}$	4.2 ± 1.8	38.5 ± 12.9
Specific loading flux (kg Nd km^{-2} yr^{-1})	Atmospheric deposition	$Q^S_{atm.}$	0.23 ± 0.03**	
	Dissolved fractions	$Q^S_{diss.}$	0.011 ± 0.002	0.026 ± 0.010
	Particulate fractions	$Q^S_{part.}$	0.07 ± 0.03	0.55 ± 0.18

* (Durrieu, 2022).
** Wet and dry depositions.

Passive fluxes of REEs from the sediments have been demonstrated to be a significant input of REEs to the oceans (Abbott et al., 2015; Haley et al., 2004; Soyol-Erdene and Huh, 2013). We applied a similar estimation suggested by Garcia-Solsona and Jeandel (2020) to determine the contribution of sedimentary outflux ($F_{sed.}$), i.e., multiplying the surface area of Toulon Bay (32 km^2) by an Nd flux across the sediment-water interface of 37 nmol m^{-2} yr^{-1} (Soyol-Erdene and Huh, 2013) and a correction factor (converting nmol to kg and m^2 to km^2) to determine the $F_{sed.}$ of 0.18 kg yr^{-1} for Toulon Bay.

The last Nd flux to the bay is the anthropogenic emissions through the discharge of treated wastewater (station 34, Fig. 8A). Dissolved Nd concentration at this station (surface) is the highest (6.1 ng L^{-1}) relative to the average concentrations of the bay of 3.1 ng L^{-1}. Although we did not collect the sample from the outlet of the discharge point, located 54 m below the surface, we will make the assumption that this concentration represents the effluent. While the treated wastewater could rise to the surface due to differences in water densities relative to seawater, this simplistic assumption does not account for the horizontal ocean currents and the mixing between two water masses. The calculation would risk underestimating the anthropogenic contributions. Nevertheless, previous data of WWTP effluents would point toward a comparable range of Nd concentrations, e.g., a median of 4.2 ng L^{-1} from 40 Canadian and American WWTPs with a similar median daily flow (11,900 m^3 per day) as the Amphora (14,700 m^3 day^{-1}) (Pinter et al., 2022). The anthropogenic loadings of Nd ($F_{anthr.}$) can be empirically estimated to be 0.03 kg yr^{-1}.

We could, therefore, determine the total fluxes of Nd to Toulon Bay (F_{TB}) of 1.1 ± 0.2 kg yr^{-1}. Of these six external sources to the water column, the fluvial dissolved flux (64.2 %), passive porewater diffusion from sediments (16.9 %), and atmospheric deposition (14.6 %) are the main processes, while anthropogenic emissions, SGD, and mobilization from particulate matter contribute 4.3 % to the mass budget. This configuration is significantly different from the mass balance of NW Mediterranean Sea, which is dominated by atmospheric deposition (44 %), porewater diffusion (30 %), river (11 %) and SGD (10 %) and dissolution from lithogenic sediments (6 %) (Garcia-Solsona and Jeandel, 2020). Such discrepancy is, however, expected given the higher ocean/watershed surface ratio in the case of the open ocean, which inherently favours higher atmospheric deposition and porewater diffusion contributions. Furthermore, in the case of this study, our river contributions are dominant due to the higher Nd concentrations of the end-member, which have been weighted by flood events that were not considered in previous studies.

With that being said, the relative contributions of each external source might be insignificant against the oceanic water advection entering the bay from the Northern Current (Ligurian Sea, Fig. 1A), given that the volume of Toulon Bay remains small relative to oceanic water masses. Previous studies have determined the water exchange time of Toulon Bay between 1.5 and 7.5 days, with an annual average of 3.4 days (Dufresne et al., 2014). From a bay volume of 850 × 10^6 m^3, we calculate the seawater influx into the bay (Q_{SW}) of 250 × 10^6 m^3 day^{-1}. Neodymium concentrations in surface seawater of the central Mediterranean Sea (3.7 ± 0.4 ng L^{-1}, $n = 10$ (Censi et al., 2004)) can be used as an end-member of the Northern Current seawater circulating from the Ionian, Tyrrhenian and Ligurian Seas. Therefore, the Nd flux associated with oceanic water mass advection ($F_{ocean} = Q_{SW} \times C_{SW} \times CF$) is 338 kg yr^{-1}. However, it is important to note that this assumption does not consider that Toulon Bay is divided by the sea dike into two unequal parts and that the little bay (90 10^6 m^3) has higher residence time than the large bay (760 10^6 m^3). Under this configuration, the inputs of Nd by external processes to the water column (1.1 ± 0.2 kg yr^{-1}) only represent 0.3 % of seawater advection. In other words, geochemical processes within a small bay area might not significantly change the oceanic Nd concentrations.

3.3.3. REE export from the coastal watersheds to the ocean

The Mediterranean Sea has a unique water exchange pattern with the Atlantic Ocean, characterized by complex hydrological and atmospheric inputs. However, the lack of understanding of the mechanisms governing the cycles of trace elements and nutrients results in imbalanced mass budgets (Garcia-Solsona and Jeandel, 2020). This previous model considered the Ebro River (net $F_R = 2.9$ ng L^{-1}) a representative fluvial input as the Rhône and Ebro Rivers dominate freshwater discharge to the NW Mediterranean Sea (Arnau et al., 2004). An extrapolation from the Ebro River leads to Nd inputs from coastal rivers of 290 ± 29 kg yr^{-1} to the NW Mediterranean Sea (Garcia-Solsona and Jeandel, 2020). The effective river loadings of the Las and Eygoutier Rivers (0.7 ± 0.2 kg yr^{-1}) are relatively small compared to the extrapolated values from the Ebro River. While the Rhône and Ebro watersheds are indeed the most significant (101,817 km^2 and 85,708 km^2) of 34 river watersheds (total surface of 230,000 km^2) of the NW Mediterranean Sea (Arnau et al., 2004), they might not represent small rivers as it has been demonstrated for 25 small rivers vs. five largest rivers in the Arctic (Brown et al., 2020). We could extrapolate the effective contribution of 32 small rivers (SR) of the Mediterranean coast to the ocean by multiplying the specific loading flux of the Las and Eygoutier River ($Q^S_{diss.}$ 0.011 to 0.026 kg Nd km^{-2} yr^{-1}, Table 1) by the watershed surface areas of 32 rivers of this region (S^{SR} = 42,475 km^2) and ϕ.

$$R^{eff-SR}_{NWMediterraneanSea} = Q^S_{diss.} \times S^{SR} \times \phi \quad (7)$$

The effective dissolved flux of small rivers (18 % in terms of surface area coverage) ranges from 140 to 327 kg yr^{-1}, which is similar to the estimated value (290 ± 29 kg yr^{-1} of Nd) based on the major Ebro River.

This observation is consistent for other trace metals (Cu and Pb) when relating the small Mediterranean coastal-draining rivers to the Rhône River (Nicolau et al., 2012).

In summary, the contributions of small fluvial systems to the oceans should be revisited in mass balance budgets of trace elements, especially during contrast seasons (base flow vs. flood, Xu et al., 2023) to constrain annual fluvial fluxes. Nonetheless, this direction would lead to increased inputs of Nd into the NW Mediterranean Sea and might not help constrain the Nd budget, as the most recent mass balance model (Garcia-Solsona and Jeandel, 2020) pointed toward missing output fluxes removing Nd (and light REEs) from the surface water column.

4. Conclusion

The karstic geology of two watersheds, along with various anthropogenic activities, governs the emissions, transport, and fates of REEs in the study area. Their annual fluvial loadings of dissolved and particulate fractions substantially vary depending on base flow or flood events; dissolved and particulate Nd concentrations increase five to seven times between the two conditions. Therefore, flow-weighted mean concentrations are undoubtedly required to integrate these extreme events into annual data, which are essential in accurately establishing the fluvial fluxes of REEs in their mass budgets.

Besides the more common Gd anomalies in river water that could be associated with wastewater of medical origins, we also observed significant La anomalies in the dissolved and atmospheric fractions, which might be associated with petroleum refining activities. However, the atmospheric source of La needs to be further constrained. Furthermore, Tb anomalies were also observed in the surface water of the large bay, covering a vast surface area receiving treated wastewater discharge.

Finally, within the two watersheds, we estimated the dissolved, particulate, and atmospheric loading of Nd and determined that atmospheric deposition was a significant input, while particulate loading was the principal output of Nd from the watershed. On the other hand, the fluxes within Toulon Bay are dominated by river dissolved fluxes (64.2 %), porewater diffusion (16.9 %), and atmospheric deposition (14.6 %), while anthropogenic emissions, submarine groundwater discharge, and mobilization from the particulate fraction remain minor. The total flux of these external sources was estimated to be 1.1 ± 0.2 kg yr^{-1}, which remains insignificant compared to the oceanic water mass advection of 338 kg Nd yr^{-1}. Although the contribution from these two watersheds (total surface area of 130 km^2) and Toulon Bay (34 km^2) remains limited with regards to the mass budget of the NW Mediterranean Sea, an extrapolation of these values to the watersheds of 32 small rivers (besides the major Rhône and Ebro Rivers) would lead to a contributions between 140 and 327 kg yr^{-1}. In other words, these results would warrant considering typically small Mediterranean rivers in the ocean's mass balance of trace elements.

CRediT authorship contribution statement

Duc Huy Dang: Writing – review & editing, Writing – original draft, Visualization, Methodology, Investigation, Funding acquisition, Formal analysis, Data curation, Conceptualization. **Gael Durrieu:** Writing – review & editing, Methodology, Formal analysis, Data curation, Conceptualization. **Wei Wang:** Writing – review & editing, Methodology, Investigation. **Dario Omanović:** Writing – review & editing, Supervision, Methodology, Investigation, Formal analysis, Data curation, Conceptualization. **Cedric Garnier:** Supervision, Resources, Project administration, Methodology, Funding acquisition, Formal analysis, Data curation, Conceptualization. **Stephane Mounier:** Writing – review & editing, Supervision, Project administration, Investigation, Funding acquisition, Formal analysis, Data curation, Conceptualization.

Declaration of competing interest

The authors declare that they have no known competing financial interests or personal relationships that could have appeared to influence the work reported in this paper.

Acknowledgements

The authors acknowledge funding from the "Agence de l'Eau Rhône Méditerranée Corse" (convention n°2016-1364) to the METFLUX project and the Natural Sciences and Engineering Research Council of Canada (NSERC) to DDH. The authors thank Dr. Karla Newman and Dr. Mathew Teeter of the Water Quality Centre (Trent University) for their help with the mass spectrometry facilities. The authors are also grateful to the METEOR technical platform of the CEM team for the carbon analyses and to the staff of the CEM team involved in sampling and maintaining the aerosol sampler. Finally, they thank IFREMER, La Seyne-sur-Mer, for hosting the aerosol collector. This work is in memory of our late colleague and mentor, Cédric Garnier (1977-2018).

Appendix A. Supplementary data

Supplementary data to this article can be found online at https://doi.org/10.1016/j.marpolbul.2025.118518.

Data availability

The data are uploaded as supplementary information

References

Abbott, A.N., Haley, B.A., McManus, J., Reimers, C.E., 2015. The sedimentary flux of dissolved rare earth elements to the ocean. Geochim. Cosmochim. Acta 154, 186–200. https://doi.org/10.1016/j.gca.2015.01.010.

Alemu, A.K., Zhang, K., Klose, L., Kraemer, D., Bau, M., 2025. Critical raw materials in river waters: First observation of lutetium microcontamination of the Isère and Rhône rivers. Southern France. Water Res. 286, 124105. https://doi.org/10.1016/j.watres.2025.124105.

Andrade, M., Soares, A.M.V.M., Solé, M., Pereira, E., Freitas, R., 2023. Assessing the impact of terbium on Mytilus galloprovincialis: Metabolic and oxidative stress responses. Chemosphere 337. https://doi.org/10.1016/j.chemosphere.2023.139299.

Arnau, B.Y.P., Liquete, C., Canals, M., 2004. River mouth plume events and their dispersal in the Northwestern Mediterranean Sea. Oceanography 17, 22–31.

Arsouze, T., Dutay, J.-C., Lacan, F., Jeandel, C., 2009. Reconstructing the Nd oceanic cycle using a coupled dynamical – biogeochemical model. Biogeosci. Discuss. 6, 5549–5588. https://doi.org/10.5194/bgd-6-5549-2009.

Bejannin, S., van Beek, P., Stieglitz, T., Souhaut, M., Tamborski, J., 2017. Combining airborne thermal infrared images and radium isotopes to study submarine groundwater discharge along the French Mediterranean coastline. J. Hydrol. Reg. Stud. 13, 72–90. https://doi.org/10.1016/j.ejrh.2017.08.001.

Bellefroid, E.J., Hood, A.V.S., Hoffman, P.F., Thomas, M.D., Reinhard, C.T., Planavsky, N.J., 2018. Constraints on paleoproterozoic atmospheric oxygen levels. Proc. Natl. Acad. Sci. USA 115, 8104–8109. https://doi.org/10.1073/pnas.1806216115.

Bolan, S., Wijesekara, H., Tanveer, M., Boschi, V., Padhye, L.P., Wijesooriya, M., Wang, L., Jasemizad, T., Wang, C., Zhang, T., Rinklebe, J., Wang, H., Lam, S.S., Siddique, K.H.M., Kirkham, M.B., Bolan, N., 2023. Beryllium contamination and its risk management in terrestrial and aquatic environmental settings. Environ. Pollut. 320. https://doi.org/10.1016/j.envpol.2023.121077.

Bozlaker, A., Buzcu-Güven, B., Fraser, M.P., Chellam, S., 2013. Insights into PM10 sources in Houston, Texas: Role of petroleum refineries in enriching lanthanoid metals during episodic emission events. Atmos. Environ. 69, 109–117. https://doi.org/10.1016/j.atmosenv.2012.11.068.

Brown, K.A., Williams, W.J., Carmack, E.C., Fiske, G., François, R., McLennan, D., Peucker-Ehrenbrink, B., 2020. Geochemistry of Small Canadian Arctic Rivers with Diverse Geological and Hydrological Settings. J. Geophys. Res. Biogeosci. 125, 1–21. https://doi.org/10.1029/2019JG005414.

Byrne, R.H., Li, B., 1995. Comparative complexation behavior of the rare earths. Geochim. Cosmochim. Acta 59, 4575–4589. https://doi.org/10.1016/0016-7037(95)00303-7.

Censi, P., Mazzola, S., Sprovieri, M., Bonanno, A., Patti, B., Punturo, R., Spoto, S.E., Saiano, F., Alonzo, G., 2004. Rare earth elements distribution in seawater and suspended particulate of the Central Mediterranean Sea. Chem. Ecol. 20, 323–343. https://doi.org/10.1080/02757540410001727954.

Chabaux, F., Riotte, J., Dequincey, O., 2003. U-Th-Ra fractionation during weathering and river transport. Uranium-series Geochemistry 52, 533–576. https://doi.org/10.2113/0520533.
Conway, T.M., Horner, T.J., Plancherel, Y., González, A.G., 2021. A decade of progress in understanding cycles of trace elements and their isotopes in the oceans. Chem. Geol. 580. https://doi.org/10.1016/j.chemgeo.2021.120381.
Crossland, C., Kremer, H.H., Linderboom, H.J., Corssland, J.I.M., Le Tissier, M.D.A., 2005. Coastal Fluxes in the Anthropocene. In: The Land-Ocean Interactions in the Coastal Zone Project of the International Geosphere-Biosphere Programme. Springer.
Dang, D.H., Lenoble, V., Durrieu, G., Omanović, D., Mullot, J.-U., Mounier, S., Garnier, C., 2015. Seasonal variations of coastal sedimentary trace metals cycling: Insight on the effect of manganese and iron (oxy)hydroxides, sulphide and organic matter. Mar. Pollut. Bull. 92, 113–124. https://doi.org/10.1016/j.marpolbul.2014.12.048.
Dang, D.H., Ma, L., Ha, Q.K., Wang, W., 2022a. A multi-tracer approach to disentangle anthropogenic emissions from natural processes in the St. Lawrence River and Estuary. Water Res. 219, 118588.
Dang, D.H., Wang, W., 2024. Reply to "Practical guidelines for representing and interpreting rare earth abundances in environmental and biological studies.". Chemosphere 360, 1–4. https://doi.org/10.1016/j.chemosphere.2024.142345.
Dang, D.H., Wang, W., Sikma, A., Chatzis, A., Mucci, A., 2022b. The contrasting estuarine geochemistry of REEs between ice-covered and ice-free conditions. Geochim. Cosmochim. Acta 317, 488–506.
Dang, D.H., Zhang, Z., Wang, W., Oursel, B., Juillot, F., Dupouy, C., Lemonnier, H., Mounier, S., 2021. Tropical mangrove forests as a source of dissolved rare earth elements and yttrium to the ocean. Chem. Geol. 576, 120278. https://doi.org/10.1016/j.chemgeo.2021.120278.
Dufresne, C., Arfib, B., Ducros, L., Duffa, C., Giner, F., Rey, V., 2020. Karst and urban flood-induced solid discharges in Mediterranean coastal rivers: The case study of Las River (SE France). J. Hydrol. 590, 125194. https://doi.org/10.1016/j.jhydrol.2020.125194.
Dufresne, C., Duffa, C., Rey, V., 2014. Wind-forced circulation model and water exchanges through the channel in the Bay of Toulon. Ocean Dyn. 64, 209–224. https://doi.org/10.1007/s10236-013-0676-3.
Durrieu, G., 2022. Apports fluviaux et atmosphériques d'éléments traces métalliques et métalloïdes en zone côtière méditerranéenne : cas de la rade de Toulon. Université de Toulon. PhD thesis.
Durrieu, G., Layglon, N., D'Onofrio, S., Oursel, B., Omanović, D., Garnier, C., Mounier, S., 2023. Extreme hydrological regimes of a small urban river: impact on trace element partitioning, enrichment and fluxes. Environ. Monit. Assess. 195. https://doi.org/10.1007/s10661-023-11622-x.
Elbaz-poulichet, F., 2005. River inputs of metals and arsenic. In: Saliot, A. (Ed.), The Mediterranean Sea. Springer, Berlin Heidelberg, pp. 211–235. https://doi.org/10.1007/b107148.
Elbaz-Poulichet, F., Guieu, C., Morley, N.H., 2001. A reassessment of trace metal budgets in the western Mediterranean Sea. Mar. Pollut. Bull. 42, 623–627. https://doi.org/10.1016/S0025-326X(01)00065-0.
Gaillardet, J., Viers, J., Dupré, B., 2003. Trace elements in river waters. In: Turekian, K. K., Holland, H.D. (Eds.), Treatise on Geochemistry. Elsevier Ltd, pp. 225–272.
Gao, S., Schwinger, J., Tjiputra, J., Bethke, I., Hartmann, J., Mayorga, E., Heinze, C., 2023. Riverine impact on future projections of marine primary production and carbon uptake. Biogeosciences 20, 93–119. https://doi.org/10.5194/bg-20-93-2023.
Garcia-Solsona, E., Jeandel, C., 2020. Balancing Rare Earth Element distributions in the Northwestern Mediterranean Sea. Chem. Geol. 532, 119372. https://doi.org/10.1016/j.chemgeo.2019.119372.
Gilbert, B., Carrero, S., Dong, W., Joe-Wong, C., Arora, B., Fox, P., Nico, P., Williams, K. H., 2023. River thorium concentrations can record bedrock fracture processes including some triggered by distant seismic events. Nat. Commun. 14, 1–8. https://doi.org/10.1038/s41467-023-37784-3.
Goldstein, S.J., Jacobsen, S.B., 1987. The Nd and Sr isotopic systematics of river-water dissolved material Implications for the sources of Nd and Sr in seawater. Chem. Geol. 66, 245–272.
Goldstein, S.J., Jacobsen, S.B., 1988. Rare earth elements in river waters. Earth Planet. Sci. Lett. 89, 35–47. https://doi.org/10.1016/0012-821X(88)90031-3.
Greaves, M.J., Statham, P.J., Elderfield, H., 1994. Rare earth element mobilization from marine atmospheric dust into seawater. Mar. Chem. 46, 255–260. https://doi.org/10.1016/0304-4203(94)90081-7.
Guigue, C., Tedetti, M., Dang, D.H., Mullot, J.U., Garnier, C., Goutx, M., 2017. Remobilization of polycyclic aromatic hydrocarbons and organic matter in seawater during sediment resuspension experiments from a polluted coastal environment: Insights from Toulon Bay (France). Environ. Pollut. 229, 627–638. https://doi.org/10.1016/j.envpol.2017.06.090.
Haley, B.A., Klinkhammer, G.P., McManus, J., 2004. Rare earth elements in pore waters of marine sediments. Geochim. Cosmochim. Acta 68, 1265–1279. https://doi.org/10.1016/j.gca.2003.09.012.
Hatje, V., Bruland, K.W., Flegal, A.R., 2016. Increases in Anthropogenic Gadolinium Anomalies and Rare Earth Element Concentrations in San Francisco Bay over a 20 Year Record. Environ. Sci. Technol. 50, 4159–4168. https://doi.org/10.1021/acs.est.5b04322.
Kim, I., Kim, G., 2011. Large fluxes of rare earth elements through submarine groundwater discharge (SGD) from a volcanic island, Jeju. Korea. Mar. Chem. 127, 12–19. https://doi.org/10.1016/j.marchem.2011.07.006.
Kulaksiz, S., Bau, M., 2007. Contrasting behaviour of anthropogenic gadolinium and natural rare earth elements in estuaries and the gadolinium input into the North Sea. Earth Planet. Sci. Lett. 260, 361–371. https://doi.org/10.1016/j.epsl.2007.06.016.
Kulaksiz, S., Bau, M., 2013. Anthropogenic dissolved and colloid/nanoparticle-bound samarium, lanthanum and gadolinium in the Rhine River and the impending destruction of the natural rare earth element distribution in rivers. Earth Planet. Sci. Lett. 362, 43–50. https://doi.org/10.1016/j.epsl.2012.11.033.
Kulkarni, P., Chellam, S., Fraser, M.P., 2007. Tracking petroleum refinery emission events using lanthanum and lanthanides as elemental markers for PM2.5. Environ. Sci. Technol. 41, 6748–6754.
Kümmerer, K., Helmers, E., 2000. Hospital effluents as a source of gadolinium in the aquatic environment. Environ. Sci. Technol. 34, 573–577. https://doi.org/10.1021/es990633h.
Langmuir, D., Herman, J.S., 1980. The mobility of thorium in natural waters at low temperatures. Geochim. Cosmochim. Acta 44, 1753–1766.
Laubier, L., 2005. Mediterranean Sea and Humans : Improving a Conflictual Partnership. In: Saliot, A. (Ed.), The Mediterranean Sea. Springer, Berlin Heidelberg, pp. 3–27. https://doi.org/10.1007/b107142.
Laukert, G., Frank, M., Bauch, D., Hathorne, E.C., Gutjahr, M., Janout, M., Hölemann, J., 2017. Transport and transformation of riverine neodymium isotope and rare earth element signatures in high latitude estuaries: A case study from the Laptev Sea. Earth Planet. Sci. Lett. 477, 205–217. https://doi.org/10.1016/j.epsl.2017.08.010.
Layglon, N., Misson, B., Durieu, G., Coclet, C., D'Onofrio, S., Dang, D.H., François, D., Mullot, J.U., Mounier, S., Lenoble, V., Omanović, D., Garnier, C., 2020. Long-term monitoring emphasizes impacts of the dredging on dissolved Cu and Pb contamination along with ultraplankton distribution and structure in Toulon Bay (NW Mediterranean Sea, France). Mar. Pollut. Bull. 156. https://doi.org/10.1016/j.marpolbul.2020.111196.
Lee, J.H., Byrne, R.H., 1993. Complexation of trivalent rare earth elements (Ce, Eu, Gd, Tb, Yb) by carbonate ions. Geochim. Cosmochim. Acta 57, 295–302. https://doi.org/10.1016/0016-7037(93)90432-V.
Lerat-Hardy, A., Coynel, A., Dutruch, L., Pereto, C., Bossy, C., Gil-Diaz, T., Capdeville, M. J., Blanc, G., Schäfer, J., 2019. Rare Earth Element fluxes over 15 years into a major European Estuary (Garonne-Gironde, SW France): Hospital effluents as a source of increasing gadolinium anomalies. Sci. Total Environ. 656, 409–420. https://doi.org/10.1016/j.scitotenv.2018.11.343.
Ma, L., Dang, D.H., Wang, Wei, Evans, R.D., Wang, Wen-xiong, 2019. Rare earth elements in the Pearl River Delta of China: Potential impacts of the REE industry on water, suspended particles and oysters. Environ. Pollut. 244, 190–201. https://doi.org/10.1016/j.envpol.2018.10.015.
McLennan, S.M., 2001. Relationships between the trace element composition of sedimentary rocks and upper continental crust. Geochem. Geophys. Geosyst. 2. https://doi.org/10.1038/scientificamerican0983-130, 2000GC000109.
Méditerranée, Métropole Toulon Provence, 2019. Rapport annuel sur le prix et la qualité du service public de l'eau et de l'assainissement.
Moreno, T., Querol, X., Alastuey, A., de la Rosa, J., Sánchez de la Campa, A.M., Minguillón, M.C., Pandolfi, M., González-Castanedo, Y., Monfort, E., Gibbons, W., 2010. Variations in vanadium, nickel and lanthanoid element concentrations in urban air. Sci. Total Environ. 408, 4569–4579. https://doi.org/10.1016/j.scitotenv.2010.06.016.
Nicolau, R., Galera-Cunha, A., Lucas, Y., 2006. Transfer of nutrients and labile metals from the continent to the sea by a small Mediterranean river. Chemosphere 63, 469–476. https://doi.org/10.1016/j.chemosphere.2005.08.025.
Nicolau, R., Lucas, Y., Merdy, P., Raynaud, M., 2012. Base flow and stormwater net fluxes of carbon and trace metals to the Mediterranean sea by an urbanized small river. Water Res. 46, 6625–6637. https://doi.org/10.1016/j.watres.2012.01.031.
Ollivier, P., Hamelin, B., Radakovitch, O., 2010. Seasonal variations of physical and chemical erosion: A three-year survey of the Rhone River (France). Geochim. Cosmochim. Acta 74, 907–927. https://doi.org/10.1016/j.gca.2009.10.037.
Pereto, C., Baudrimont, M., Coynel, A., 2024. Global natural concentrations of Rare Earth Elements in aquatic organisms: Progress and lessons from fifty years of studies. Sci. Total Environ. 922. https://doi.org/10.1016/j.scitotenv.2024.171241.
Phillips, J., Russell, M., Walling, D., 2000. Time-integrated sampling of fluvial suspended sediment: a simple methodology for small catchments. Hydrol. Process. 14, 2589–2602.
Pinter, J., Jones, B.S., Vriens, B., 2022. Loads and elimination of trace elements in wastewater in the Great Lakes basin. Water Res. 209, 117949. https://doi.org/10.1016/j.watres.2021.117949.
Rabiet, M., Brissaud, F., Seidel, J.L., Pistre, S., Elbaz-Poulichet, F., 2009. Positive gadolinium anomalies in wastewater treatment plant effluents and aquatic environment in the Hérault watershed (South France). Chemosphere 75, 1057–1064. https://doi.org/10.1016/j.chemosphere.2009.01.036.
Rétif, J., Zalouk-Vergnoux, A., Briant, N., Poirier, L., 2023. From geochemistry to ecotoxicology of rare earth elements in aquatic environments: Diversity and uses of normalization reference materials and anomaly calculation methods. Sci. Total Environ. 856. https://doi.org/10.1016/j.scitotenv.2022.158890.
Rousseau, T.C.C., Sonke, J.E., Chmeleff, J., Van Beek, P., Souhaut, M., Boaventura, G., Seyler, P., Jeandel, C., 2015. Rapid neodymium release to marine waters from lithogenic sediments in the Amazon estuary. Nat. Commun. 6, 1–8. https://doi.org/10.1038/ncomms8592.
Rudnick, R., Gao, S., 2003. Composition of the continental crust. In: Turekian, K.K., Holland, H.D. (Eds.), Treatise on Geochemistry. Elsevier Ltd, pp. 1–64.
Shimamura, T., Iwashita, M., Iijima, S., Shintani, M., Takaku, Y., 2007. Major to ultra trace elements in rainfall collected in suburban Tokyo. Atmos. Environ. 41, 6999–7010. https://doi.org/10.1016/j.atmosenv.2007.05.010.
Soyol-Erdene, T.O., Huh, Y., 2013. Rare earth element cycling in the pore waters of the Bering Sea Slope (IODP Exp. 323). Chem. Geol. 358, 75–89. https://doi.org/10.1016/j.chemgeo.2013.08.047.

Sugiyama, N., 2022. Direct Analysis of Ultratrace Rare Earth Elements in Enviromental Waters by ICP-QQQ (Agilent Application note).

Szramek, K., McIntosh, J.C., Williams, E.L., Kanduc, T., Ogrinc, N., Walter, L.M., 2007. Relative weathering intensity of calcite versus dolomite in carbonate-bearing temperate zone watersheds: Carbonate geochemistry and fluxes from catchments within the St. Lawrence and Danube river basins. Geochemistry, Geophys. Geosystems 8. https://doi.org/10.1029/2006GC001337.

Tagliabue, A., Weber, T., 2024. Novel Insights into Ocean Trace Element Cycling from Biogeochemical Models. Oceanography 37, 131–141.

Tessier, E., Garnier, C., Mullot, J.-U., Lenoble, V., Arnaud, M., Raynaud, M., Mounier, S., 2011. Study of the spatial and historical distribution of sediment inorganic contamination in the Toulon bay (France). Mar. Pollut. Bull. 62, 2075–2086. https://doi.org/10.1016/j.marpolbul.2011.07.022.

Wang, W., Ma, L., Evans, R.D., Babechuk, M.G., Dang, D.H., 2022. Quantification of Re and four other trace elements (Ag, Cd, Pd, Zn) in certified reference materials and natural waters. J. Anal. At. Spectrom. 37, 1471–1483. https://doi.org/10.1039/d2ja00073c.

Wang, X., Barrat, J.A., Bayon, G., Chauvaud, L., Feng, D., 2020. Lanthanum anomalies as fingerprints of methanotrophy. Geochemical Perspect. Lett. 14, 26–30. https://doi.org/10.7185/GEOCHEMLET.2019.

Xu, A., Hathorne, E., Laukert, G., Frank, M., 2023. Overlooked riverine contributions of dissolved neodymium and hafnium to the Amazon estuary and oceans. Nat. Commun. 14, 1–12. https://doi.org/10.1038/s41467-023-39922-3.

Zhu, Z., Liu, C.Q., Wang, Z.L., Liu, X., Li, J., 2016. Rare earth elements concentrations and speciation in rainwater from Guiyang, an acid rain impacted zone of Southwest China. Chem. Geol. 442, 23–34. https://doi.org/10.1016/j.chemgeo.2016.08.038.